Conversion of Polypropylene to Light Olefins by HMFI Catalysts Below Pyrolytic Temperature

Catalytic, Spectroscopic, and Theoretical Studies

Ando, Yuriko; Miyakage, Takumi; Anzai, Akihiko; Huang, Mengwen; Ait El Fakir, Abdellah; Toyao, Takashi; Kolganov, Alexander A.; Pidko, Evgeny A.; Shimizu, Ken Ichi; More Authors

DOI
10.1021/acs.jpcc.4c06925

Publication date
2025

Document Version
Final published version

Published in
Journal of Physical Chemistry C

THE JOURNAL OF PHYSICAL CHEMISTRY C
A JOURNAL OF THE AMERICAN CHEMICAL SOCIETY

pubs.acs.org/JPCC

Article

Conversion of Polypropylene to Light Olefins by HMFI Catalysts below Pyrolytic Temperature: Catalytic, Spectroscopic, and Theoretical Studies

Published as part of The Journal of Physical Chemistry C special issue "Spectroscopic Techniques for Renewable Energy".

Yuriko Ando, Takumi Miyakage, Akihiko Anzai,* Mengwen Huang, Abdellah Ait El Fakir, Takashi Toyao, Yuta Nakasaka, Alisa Phuekphong, Makoto Ogawa, Alexander A. Kolganov, Evgeny A. Pidko, and Ken-ichi Shimizu*

Cite This: https://doi.org/10.1021/acs.jpcc.4c06925

Read Online

ACCESS | Metrics & More | Article Recommendations | Supporting Information

ABSTRACT: Plastic waste is a major environmental issue; converting it directly into valuable chemicals by using catalysts is a promising alternative to plastic recycling. Here, we report the selective catalytic cracking of polypropylene (PP), a typical commodity plastic, to high-value light olefins (C_2−C_5), below pyrolytic temperature (290 °C) and without external hydrogen supply, by using zeolite catalysts. Among the H^+-form zeolites with different structures, HMFI showed the highest yields of light hydrocarbons (C_2−C_5), of which light olefins (C_2−C_5) were the major products. The HMFI-catalyzed PP conversion was applicable to the upcycling of a model PP waste, resulting in a 61.9% light hydrocarbon yield. The results of catalytic and *in situ* IR experiments using model HMFI catalysts with a small amount of external Brønsted acid sites suggested that the Brønsted acid sites on the external surface of HMFI are indispensable for the PP conversion and are posited to be the active sites for the cracking of PP into short-chain (oligomeric) hydrocarbon species as intermediate products. Density functional theory analyses were conducted to determine plausible reaction pathways by adopting 2,4-dimethylheptene as the shortest unit of the oligomeric species. The obtained results show that the β-scission of 2,4-dimethylheptene by Brønsted acid sites yields isobutene and propylene (or a propyl alkoxide group) via carbocation intermediates with an activation energy below 118 kJ mol^{-1}. *Operando* UV−vis and IR experiments under the reaction conditions, combined with *ex situ* ^{1}H NMR and ^{13}C NMR analyses of the spent catalyst, show that some of the olefins are further converted to light or heavy aromatics (coke deposit), probably via carbenium ion species.

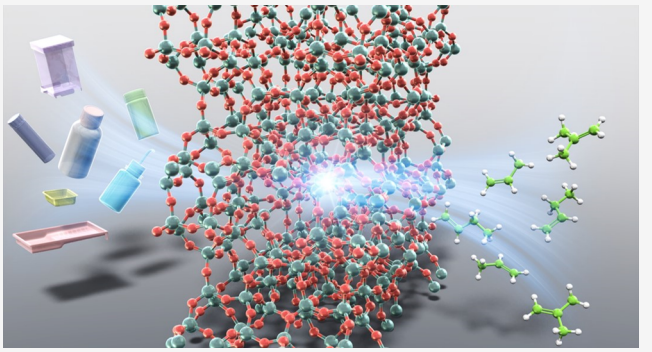

1. INTRODUCTION

Plastic pollution has become a global issue that needs to be addressed urgently. Globally, over 250 million tons of plastic waste are generated each year, and only approximately 20% of the waste plastic is recycled.[1,2] There are several solutions to the plastic waste problem, including reducing plastic usage, developing sustainable alternatives, and recycling plastic wastes.[3−12] Current recycling techniques rely mostly on mechanical processes, but mechanically recycled plastics often exhibit inferior properties compared to virgin plastics.[13] On the other hand, chemical recycling is an alternative approach to the plastic waste issue that reproduces original monomers or upcycle waste plastics into high-value chemicals and fuels.[10,14−29] Despite its potential benefits, the chemical recycling of plastic waste must overcome several issues.

Polyolefins are the most widely used plastics; hence, the conversion of polyolefins into useful monomers or other chemical feedstocks would be one of the key technologies to solve the waste plastic issue.[4,30−32] However, the cleavage of $C(sp^3)$−$C(sp^3)$ bonds in polyolefins such as polyethylene (PE) and polypropylene (PP) requires harsh reaction conditions and large amounts of energy, resulting in the production of a mixture of various products. A recent report on the pyrolysis of PE and

Received: October 12, 2024
Revised: December 21, 2024
Accepted: December 23, 2024

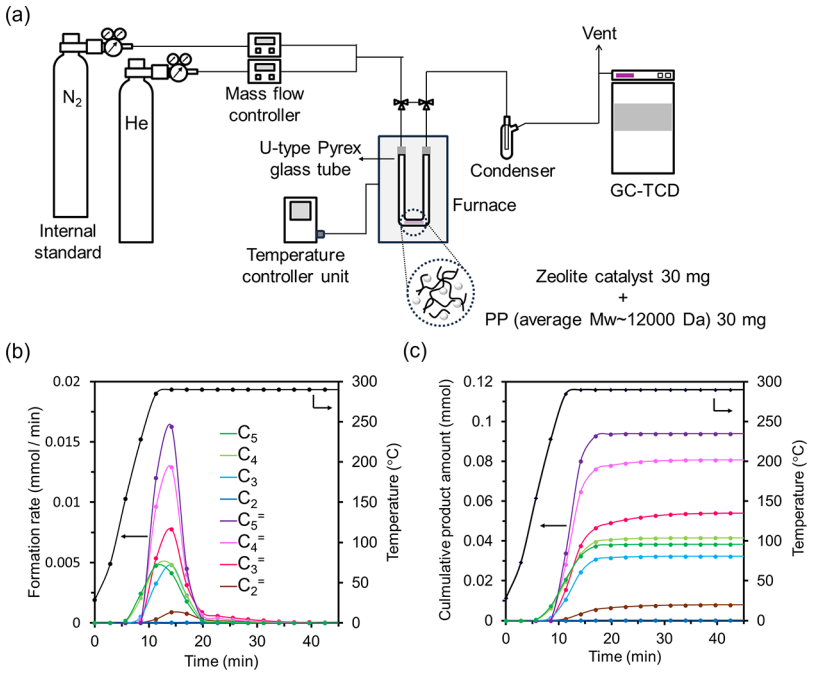

Figure 1. (a) Schematic illustration of the experimental setup for PP conversion. Typical time courses of (b) the rates of product formation and (c) cumulative product formation under temperature ramping conditions: 25−290 °C, 20 °C min^{-1}, 10% N_2/He (10 mL min^{-1}), 0.03 g of HMFI11, 0.03 g of PP.

PP showed that the catalyst-free pyrolysis of PE and PP gave mainly waxy products at temperatures of 400−550 °C and gas and oil at temperatures of 700 °C.[5] Earlier reports on catalytic depolymerization using solid acid catalysts (such as aluminosilicate zeolite) succeeded in suppressing the wax formation at high temperatures (e.g., >450 °C), but rapid coke formation resulted in rapid catalyst deactivation.[33−44]

Recently, a large number of papers have been reported on the selective formation of hydrocarbons through the depolymerization of PE and PP by a low-temperature catalytic method under H_2.[14,15,21,45−53] Most of these methods utilized transition-metal-based catalysts such as supported Pt nanoparticle catalysts.[54] From an economical viewpoint, catalysts consisting of typical inexpensive and earth-abundant elements should be used in the industrial polyolefin recycling process. In this context, the low-temperature depolymerization of PE by a thin-layer HMFI catalyst developed by the group of Xiao[25] is of significance. This method selectively converted PE to olefins with a narrow distribution (C_3−C_6 olefins). Lee et al. reported that commercial HMFI catalysts are effective for the depolymerization of polyethylene under H_2.[55] Recently, Cargnello et al.[56] and Zhang et al.[57] have independently reported the conversion of PE into alkyl aromatics by demonstrating that SiO_2−Al_2O_3 or HMFI catalysts performed well in the absence of external H_2 using a batch reactor. These studies demonstrated a new polyolefin recycling process with inexpensive catalysts without external H_2 at 280 °C, which may be suitable for economical polyolefin recycling in industry. Despite these advancements, very few studies have succeeded in the selective production of the monomers of polyolefins such as ethylene and propylene by catalytic depolymerization of polyolefins in the absence of external H_2 below the pyrolytic temperature of PP. Also, previous reports on theoretical and *in situ* or *operando* spectroscopic analyses of the low-temperature PP depolymerization mechanism over zeolites are limited;[58] the lack of fundamental understanding hinders further improvement of the catalytic properties.

We report herein the selective depolymerization of PP into C_2−C_4 hydrocarbons (especially, light olefins) over commercial HMFI catalysts in the absence of solvent or external H_2 at 290 °C. Based on the results for model HMFI catalysts with a small amount of external Brønsted acid sites, the role of external acid sites will be discussed. *Operando* IR and UV−vis spectroscopic experiments under catalytic conditions show dynamic changes in the surface carbon-containing species, as well as the formation rates of the gas-phase products (light hydrocarbons). Combining these results with computational studies on the reaction coordinates for the cracking of a model intermediate species (2,4-dimethylheptene) provides molecular insights into the zeolite-catalyzed upgrading of PP to light olefins.

2. EXPERIMENTAL SECTION

2.1. Materials. Polypropylene (PP, average M_w ∼ 12 000 Da) was purchased from Sigma-Aldrich Co., Ltd. NH_4−MFI (Si/Al = 11.15), NH_4−Chabazite (Si/Al = 11.15), NH_4−Ferrierite (Si/Al = 9), NH_4−β (Si/Al = 8.76), H−Mordenite (Si/Al = 9.1), and H−Y-type zeolite (Si/Al = 5.3) were provided by Tosoh Co. Ltd.

2.2. Catalyst Preparation. NH_4^+-type zeolites (NH_4−MFI, NH_4−Chabazite, NH_4−Ferrierite, and NH_4−β) were converted to H^+-type by calcination at 500 °C for 1 h under an air flow using a heating rate of 10 °C/min; these catalysts were denoted as HMFI, HCHA, HFER, and Hβ, respectively. H^+-type zeolites (H−Mordenite and H−Y-type zeolite) were used without further treatment; these catalysts were denoted as HMOR and HY, respectively. Tetraethoxysilane (TEOS)-treated HMFI11 (HMFI11-T) was prepared by refluxing a mixture of HMFI11 (2 g, dried at 100 °C) and TEOS (0.24 mmol) in *n*-hexane (50 mL) for 1 h, followed by filtering and washing with toluene and acetone, drying at 100 °C for 1 h, and calcining at 600 °C for 1 h.

https://doi.org/10.1021/acs.jpcc.4c06925
J. Phys. Chem. C XXXX, XXX, XXX−XXX

Next, TEOS (0.24 mmol) was added to this catalyst in *n*-hexane (50 mL); the solution was refluxed, washed, and dried as before. HMFI140-L zeolite was hydrothermally synthesized using a water/surfactant/organic solution.[59] A solution containing tetraethylorthosilicate (Si source), aluminum isopropoxide (Al source), tetrapropyl ammonium hydroxide (structure-directing agent), polyoxyethylene-(15)-oleyl ether, and cyclohexane was poured into a Teflon-lined stainless steel autoclave and heated to 150 °C for 72 h. The obtained zeolite was washed well with 2-propanol and distilled water, followed by drying in an air atmosphere at 110 °C and then calcining at 550 °C for 12 h. The Na^+-form type zeolite was converted to the NH_4^+-type zeolite by exchanging with NH_4NO_3 three times, and the NH_4^+-type zeolite was converted to the H^+-type by calcination at 500 °C for 1 h under air.

2.3. Catalytic Testing. Catalytic tests were performed at atmospheric pressure using a fixed-bed flow reactor (U-shaped Pyrex glass tube) with an inner diameter of 3 mm. The catalyst powder (typically 30 mg) mixed with 30 mg of PP was placed in the bottom of the reactor, which was then purged with He (30 °C, 0.5 h). The temperature was measured by a thermocouple with a tip at the bottom of the reactor. Under flowing 10% N_2/He (flow rate of 10 mL min^{-1}), the catalyst bed was heated to the reaction temperature (typically 290 °C) with a ramping rate of 20 °C min^{-1}, and then maintained at 290 °C (±10 °C). The products in the outlet gas were analyzed using an online gas chromatograph (GC) with a TCD detector (Agilent 990 Micro GC) using N_2 as internal standard. Multiplying the mole fraction of each product by the molar N_2 feed rate provides an estimation of product formation ($\dot{n}_{c_i}$). In a separate experiment for the analysis of liquid-phase products, the outlet gas of the reactor was connected to a cold bath (0 °C) and dissolved in acetone. After the reaction, decane was added to the products trapped in acetone as an internal standard for analysis by a gas chromatography−flame ionization detector (GC-2014 FID, Shimadzu) equipped with UA-1 column. Integrating the molar flow rate ($\dot{n}_{c_i}$) of each species using the trapezoidal rule within a flow reaction profile (see Figure 1(b)) affords the total moles of product formed (n_{c_i}) for a given experiment (see Figure 1(c)).

We can then estimate the overall fractional yield of c_i using this cumulative quantity according to eq 1

$$Y_{C_i} = \frac{n_{c_i} \times (\text{carbon number of the product})}{n_{PP}} \quad (1)$$

where n_{PP} is calculated by dividing the mass of PP by the molecular weight of its monomer, propylene (42), and then multiplying the result by 3, which is the number of carbon atoms per monomer in PP, according to eq 2

$$n_{PP} = (\text{weight of PP}) \times \frac{3}{42} \quad (2)$$

Equation 1 becomes eq 3

$$Y_{C_i} = \frac{n_{c_i} \times (\text{carbon number of the product})}{\text{weight of PP}} \times \frac{42}{3} \quad (3)$$

The coke yield was calculated by dividing the moles of CO_2 produced during a temperature-programmed oxidation (TPO) experiment of the spent catalyst by the original moles of PP.

2.4. Catalyst Characterization. Infrared (IR) spectra were measured in the transmission-mode JASCO FT/IR-4200 spectrometer (MCT detector) by accumulating 20 scans at a resolution of 4 cm^{-1}. Prior to recording the spectra, the self-supported thin disk of sample was prepared by mixing the pre-ground PP (ca. 5 mg) with ca. 45 mg of zeolite powder by mortar and pestle and then pressing the mixture in a 10 mm diameter die under a total force of 40 MPa for 30 s. The disk was placed in a flow-type IR cell (with CaF_2 windows) connected to a flow reaction system (total flow: 100 mL min^{-1}).

After dehydration of the sample disk at 500 °C under He flow, a background spectrum was taken under He at 200 °C. Then, 2,6-di-*tert*-butylpyridine (DTBPy, 0.3 mmol g^{-1}) was introduced to the sample, followed by purging with He for 1800 s and by an IR measurement of adsorbed DTBPy at 200 °C.

In situ IR experiments under the catalytic conditions were performed by using the above apparatus. The catalyst powder was mixed with PP in specified proportions and placed in the bottom of the reactor, which was purged with He (30 °C, 0.5 h). The mixed powder was pelletized into a 50 mg self-supported thin disk and placed in a flow-type IR cell (with CaF_2 windows) connected to a flow reaction system (total flow: 50 mL min^{-1}). A schematic illustration of the apparatus is shown in Figure S1.

In situ diffuse reflectance UV−vis experiments under catalytic conditions were carried out by a JASCO V-750 UV−vis spectrometer. A mixture of PP and a catalyst powder sample (30−50 mg) mixed in specified proportions was placed in the *in situ* cell (JASCO HISV-728 in Figure S1) with a quartz window. The inlet of the cell was connected to the gas flow system and a flow reaction system (total flow: 50 mL min^{-1}). The background spectrum was obtained by using $BaSO_4$. Reflectance data were converted to pseudo-absorbance using the Kubelka−Munk (KM) function. For selected *in situ* experiments, the outlet gas of the *in situ* cell was connected to a GC-TCD instrument (Agilent 990 Micro GC). A schematic illustration of the apparatus is shown in Figure S2.

^1H and ^{13}C magic-angle spinning NMR measurements were carried out on a Bruker DSX-300 spectrometer operating at 300 MHz with a 4 mm rotor. Dipolar decoupling measurement was used for ^1H and cross-polarization measurement was used for ^{13}C.

Scanning electron microscopy (SEM) images were obtained using a JSM-7400F (JEOL Co., Ltd.).

2.5. Computational Details. All calculations were carried out using periodic density functional theory (DFT) simulations performed with the CP2K 2023.2 software package.[60] The structure of the MFI zeolite was obtained from the International Zeolite Association database.[61] The parameters for the MFI structure were set to a = 20.090 Å, b = 19.738 Å, and c = 13.142 Å. The T12 silicon of the MFI model was chosen for replacement with an Al atom based on its stability.[62] The generalized gradient approximation (GGA) with the Perdew−Burke−Ernzerhof (PBE) functional was used to describe the exchange-correlation energy, including empirical dispersion corrections by Grimme's D3 scheme with Becke−Johnson damping.[63−65] The periodic Poisson solver was utilized in combination with Goedecker−Teter−Hutter (GTH) pseudopotentials.[66,67] A cutoff of 450 Ry and a relative cutoff of 50 Ry were applied for the plane-wave basis set. A DZVP-MOLOPT-SR-GTH basis set was used. The orbital transformation (OT) method with direct inversion in the iterative subspace (DIIS) minimizer and full single-inverse preconditioner was employed to accelerate self-consistent field (SCF) convergence.[68]

The structural optimization was performed with the Broyden−Fletcher−Goldfarb−Shanno (BFGS) optimizer.[69−72]

https://doi.org/10.1021/acs.jpcc.4c06925
J. Phys. Chem. C XXXX, XXX, XXX−XXX

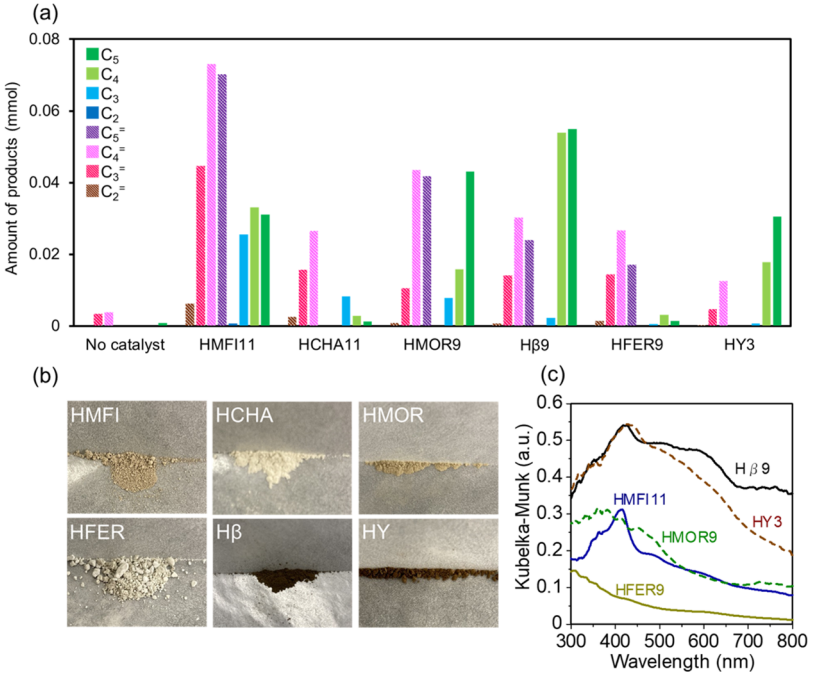

Figure 2. (a) Amounts of products for the conversion of PP (0.03 g) by various zeolites (0.03 g) at 280 °C under 10% N_2/He. (b) Photographs and (c) UV−vis spectra of the catalysts after the reaction.

The SCF convergence criterion was set to $1.0 \times 1 \times 10^{-6}$ Hartrees with a maximum of 300 SCF iterations.

The climbing-image nudged-elastic-band (CI-NEB) method was employed to locate the transition state.[73] The climbing process was initiated after five initial NEB steps. The number of replicas was set to 8. After the CI-NEB, the structural optimization for locating the transition state was performed with the dimer method[74,75] and the conjugate gradient (CG) optimizer.[76] The maximum number of steepest descent steps for the CG optimizer was set to zero, and a two-point line-search method was employed with a maximum allowed step of 0.01 Bohr.

Vibrational analysis was performed using the finite differences method with a displacement parameter (DX) of 0.01 Å and fully periodic boundary conditions. The calculations considered only the vibrational frequencies of the extraframework atoms, whereas all other atoms were fixed.

In this study, the vibrational modes and zero-point vibrational energy (E_{ZPE}) enthalpies, entropies, and thermal corrections were calculated to analyze the energy changes in catalytic reactions. E_{ZPE} was determined using eq 4[77,78]

$$E_{ZPE} = E_{elec} + E_{ZPV} \tag{4}$$

Here, E_{ZPV} was calculated based on the vibrational mode wavenumbers (ω_i) as eq 5

$$E_{ZPV} = N_a \sum_i \frac{1}{2} h\nu_i = 0.72R \sum_i \omega_i \tag{5}$$

The vibrational partition functions considered only the proton on the zeolite and the species adsorbed on the zeolite.

The enthalpy (H) was evaluated using eq 6

$$H = U + pV \tag{6}$$

where the internal energy (U) is defined as eq 7

$$U = E_{ZPE} + E_{therm} \tag{7}$$

Here, E_{therm} represents the sum of translational (E_{trans}), rotational (E_{rot}), and vibrational (E_{vib}) energy components (eq 8)

$$E_{therm} = E_{trans} + E_{rot} + E_{vib} \tag{8}$$

These components were calculated according to eqs 9−11 as follows:

For gas-phase molecules

$$E_{trans} = E_{rot} = \frac{3}{2}RT \tag{9}$$

For zeolite systems

$$E_{trans} = E_{rot} = 0 \tag{10}$$

The vibrational energy (E_{vib}) was computed by using eq 11

$$E_{vib} = R \sum_i \frac{h\nu_i}{k(e^{(h\nu_i/kT)} - 1)} = R \sum_i \frac{1.44\omega_i}{(e^{(1.44\omega_i/T)} - 1)} \tag{11}$$

Entropy was determined with eqs 12−16.

The entropy (S) was determined according to eq 12

$$S = S_{trans} + S_{rot} + S_{vib} \tag{12}$$

Each term is defined according to eqs 13−16

$$S_{vib} = R \sum_i \left[\frac{h\nu_i}{kT(e^{(h\nu_i/kT)} - 1)} - \ln(1 - e^{(-h\nu_i/kT)}) \right] = R \sum_i \left[\frac{1.44\omega_i}{T(e^{(1.44\omega_i/T)} - 1)} - \ln(1 - e^{(-1.44\omega_i/T)}) \right] \tag{13}$$

$$S_{trans} = R\left\{ \ln\left[\left(\frac{2\pi MkT}{h^2} \right)^{3/2} \frac{V^\circ}{N_A} \right] + \frac{5}{2} \right\} \tag{14}$$

https://doi.org/10.1021/acs.jpcc.4c06925
J. Phys. Chem. C XXXX, XXX, XXX−XXX

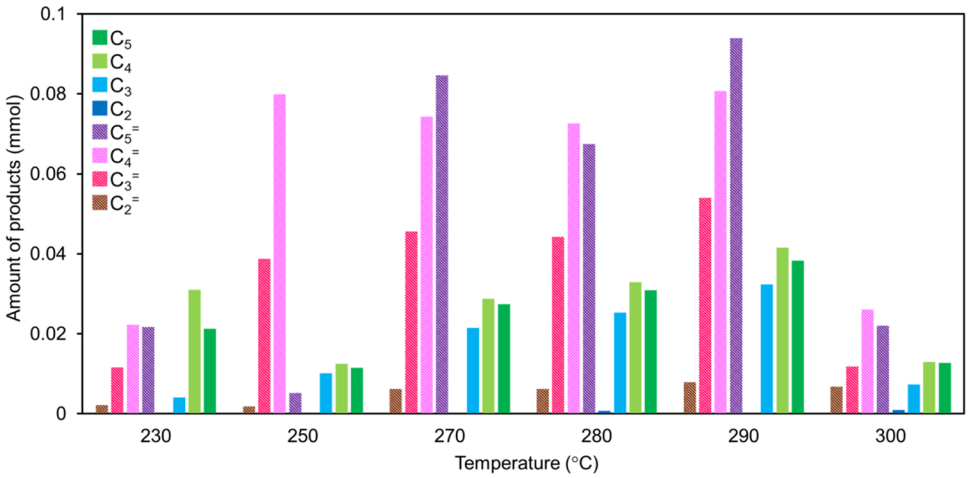

Figure 3. PP conversion by HMFI11 at different temperatures. Conditions: 10% N_2/He (10 mL min^{-1}), 0.03 g of catalyst, and 0.03 g of PP.

Under the assumption of an ideal gas, $\frac{V^o}{N_A}$ in the term in brackets in the eq 14 can be replaced by $\frac{k_B T}{P^o}$, where k_B is the Boltzmann constant and P^o is the standard pressure (1 atm).

For three-dimensional rotation

$$S_{rot}(3D) = R\left\{\ln\left[\frac{\sqrt{\pi I_A I_B I_C}}{\sigma}\left(\frac{8\pi^2 kT}{h^2}\right)^{3/2}\right] + \frac{3}{2}\right\} \quad (15)$$

For one-dimensional rotation

$$S_{rot}(1D) = R\left\{\ln\left[\frac{\sqrt{\pi I_A}}{\sigma}\left(\frac{8\pi^2 kT}{h^2}\right)^{1/2}\right] + \frac{1}{2}\right\} \quad (16)$$

where I_X is the principal symmetry moments and σ is an external symmetry number. The enthalpy, entropy, and thermal corrections to the electronic energy for gas-phase species were determined using the THERMOCHEMISTRY keyword implemented in CP2K, along with the necessary parameters such as V^o. Free energies were calculated at 563 K, based on the experimental conditions of the kinetic studies. The spurious frequencies' contributions to the enthalpy and entropy, were neglected by replacing imaginary frequencies under 100i cm^{-1} with 50 cm^{-1} for all structures to give consistent results.[79]

3. RESULTS AND DISCUSSION

3.1. Catalyst Screening for PP Conversion. Figure 1(a) shows a schematic illustration of the apparatus and typical catalytic results for PP conversion. The reactor (U-type glass tube) containing a physical mixture of 0.03 g of HMFI11 and 0.03 g of PP was heated from 25 to 290 °C (20 °C min^{-1}) under flowing N_2/He. Based on GC analysis of the outlet gas, the rates of product formation are plotted as a function of time. The formation of hydrocarbons (C_2−C_5 alkanes and monoolefins) was observed above 230 °C, and the formation rates reached a maximum after the temperature reached 290 °C, as shown in Figure 1(b). The plot for the product formation rates versus time is converted to the cumulative amount of the hydrocarbons versus time in Figure 1(c). Based on this data, the yields of hydrocarbon, as shown in the bar graph in the figure, were calculated. Detailed product distribution is shown in Figure S3 (Supporting Information).

The above experiments and analyses for the PP conversion by different zeolite catalysts at 280 °C gave the amounts of several light hydrocarbons in millimolar quantities in Figure 2(a). A blank experiment, without a catalyst, gave little amount of hydrocarbons. The presence of zeolite catalysts increased the yields of hydrocarbons. Among the H^+-type zeolites screened, HMFI11 showed the highest production of hydrocarbons. Light olefins, including ethylene ($C_2^=$), propylene ($C_3^=$), butenes ($C_4^=$), and pentenes ($C_5^=$) were the major products. For all catalysts tested, the yields of methane and liquid hydrocarbons (>C_6) were below the detection limit of GC analyses. Photographs and UV−vis spectra of the catalysts after the reaction are shown in Figure 2(b) and (c), respectively. After the reaction, Hβ9 was colored black, and HY3 was colored dark brown. The UV−vis spectra Hβ9 and HY3 showed strong bands assignable to small polyaromatics (around 600 nm) and large polyaromatics (>750 nm).[80] HMFI11 and HMOR9 were colored light brown, and these catalysts showed weak UV−vis bands at 600 and 750 nm. The results indicate that the PP conversion reaction on these catalysts leads to coke formation and a relatively large amount of coke is deposited on Hβ9 and HY3.

Next, we studied the effect of reaction temperatures on the product yields for PP conversion by HMFI11 (Figure 3). The amount of products showed a volcano-shaped dependence on the temperature, and the highest amounts of hydrocarbons and olefins were obtained at 290 °C. The calculated product yields based on the amount of products over HMFI11 are also shown in Figure S4. The yield of unknown decreased, while the yield of C_2−C_5 gas products increased from 230 to 290 °C. This indicates that in the lower temperature around 230 °C, PP is first cracked into shorter-chain oligomers (having carbon numbers of at least C_6 or more, which were undetectable by micro-GC), and then cracked at higher temperatures to produce C_2−C_5 gas products. On the other hand, at 300 °C, the proportion of unknown increased significantly, and the yield of C_2−C_5 gas products dropped sharply, which is probably related mainly to the coking.[81]

Figure 4 compares the product yields for PP conversion at 290 °C by HMFI catalysts with various Si/Al ratios. HMFI11 and HMFI150 gave high yields. Hereafter, HMFI11 and HMFI150 were used as standard catalysts for further studies.

The present method using the HMFI11 catalyst was applied to the upcycling of a model PP waste (Figure 5). A commercial

https://doi.org/10.1021/acs.jpcc.4c06925
J. Phys. Chem. C XXXX, XXX, XXX−XXX

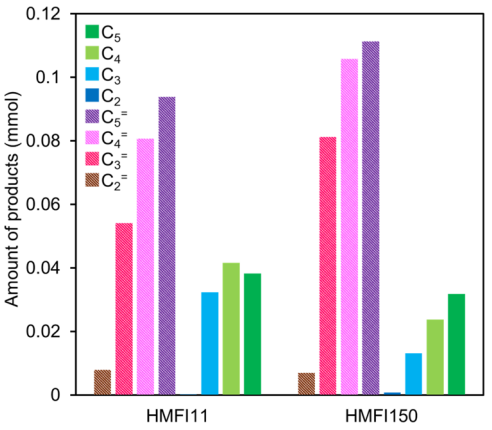

Figure 4. PP conversion by HMFI catalysts with different Si/Al ratios. Conditions: 290 °C, 10% N_2/He (10 mL min^{-1}), 0.03 g of catalyst, and 0.03 g of PP.

PP container (30 mg), cut into <3 mm sized pieces, and HMFI11 powder (30 mg) were placed in the glass reactor and heated to 290 °C under the same conditions as in Figure 4; Figure 5(a) represents a schematic of this process with pictures of the materials at each step. Light hydrocarbons (C_2−C_5) were obtained in 1 h, and the total yield of the hydrocarbons was 61.9%. Among them, the yield of light olefins was 31.4% and the olefin-to-paraffin ratio was almost unity. The coke yield was estimated to be 28.1%. Figure 5(b) presents a bar graph of these results. The result demonstrates that the present method can be applicable to the upcycling of PP waste to light olefins.

3.2. Effects of External Acid Sites and Zeolite Size. Zheng and co-workers established that the bridging hydroxyl groups (Brønsted acid sites) on external surfaces (including pore mouth regions) of HMFI samples could be passivated by chemical liquid deposition (CLD) with tetraethoxysilane (TEOS).[82] Adopting a procedure similar to that of TEOS treatment in the literature, we prepared the TEOS-treated HMFI11 (named HMFI11-T), and compared the relative amount of the Brønsted acid sites on the external surfaces and the total amount of the Brønsted acid sites in HMFI11 and HMFI11-T by IR spectroscopy of the adsorbed 2,6-di-tert-butylpyridine (DTBPy) and pyridine (Py). Figure 6(a) shows the IR spectra of Py adsorbed on HMFI11 and HMFI11-T at 200 °C. The band at 1542 cm^{-1} is characteristic of the PyH^+ ion, that is, Py protonated by the Brønsted acid sites on both the external and internal surfaces of the zeolites. Figure 6(b) shows the IR spectra of adsorbed DTBPy on the two catalysts at 200 °C. The band at 1614 cm^{-1} is assigned to the ring vibration of the $DTBPyH^+$ ion.[82] The intensity of the band at 1614 cm^{-1} corresponds to the relative amount of the Brønsted acid sites on the external surfaces, and its intensity was much stronger on HMFI11 than on HMFI11-T. Thus, the TEOS treatment passivated the Brønsted acid sites on both the external and internal surfaces, but the acid sites on the external surfaces were more preferentially passivated. Figure 6(c) compares product yields for PP conversion by HMFI11 and HMFI11-T. The result shows that the TEOS treatment significantly decreases the total yield of hydrocarbons. Combined with the IR results, these data verify that Brønsted acid sites on the external surfaces of the catalysts play significant roles in the conversion of PP to light hydrocarbons.

Next, we studied the effect of zeolite crystalline size on the acidic and catalytic properties. According to a well-established method, a large crystalline HMFI sample with a Si/Al ratio of 140 (HMFI140-L) was prepared.[83] Figure 7(a,b) compares SEM images of HMFI140-L and a standard catalyst (HMFI150) with a similar Si/Al ratio (Si/Al = 150). The standard HMFI150 catalyst is composed of small crystals with a size range of 0.2−0.3 μm, whereas the HMFI140-L catalyst is composed mainly of large rectangular crystals with a size range of 5−20 μm. The IR results for Py adsorbed on these samples (Figure 7(c)) show that HMFI140-L has a larger amount of the total Brønsted acid sites than HMFI150 has. In contrast, the IR results of the samples with adsorbed DTBPy (Figure 7(d)) show that HMFI140-L has a significantly lower amount of Brønsted acid sites on external surfaces than does HMFI150, suggesting that most Brønsted acid sites on HMFI140-L are on the internal surface. The catalytic results for the PP conversion by these catalysts (Figure 7(e)) show that HMFI140-L is nearly inactive for the PP conversion to light hydrocarbons under the conditions in which HMFI150 gave a high amount of light hydrocarbons. The result demonstrates that the HMFI catalyst with a larger crystalline size gives significantly lower catalytic activity for the PP conversion to light hydrocarbons.[28] Therefore, from considering the results in Figure 6 and the IR results of these catalysts, we conclude that Brønsted acid sites on external surfaces are indispensable for this reaction.

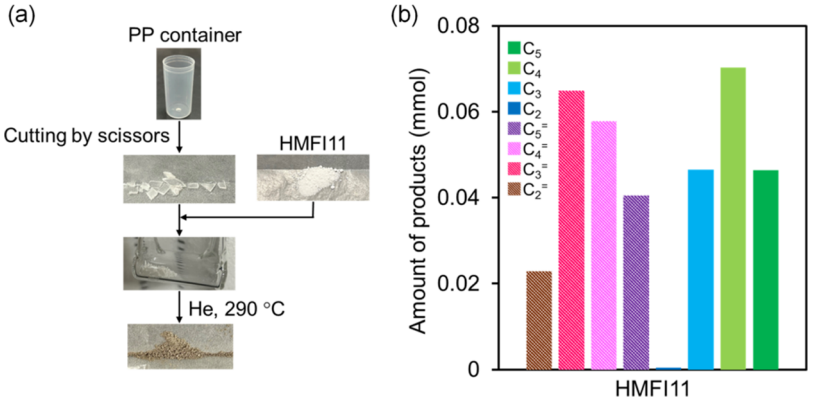

Figure 5. (a) Schematic of the process with pictures of the PP container initially and the reactants or products at each stage of processing. (b) Amounts of products for pyrolysis of a model PP waste by HMFI11. Reaction conditions: 30 mg of HMFI11, 30 mg of PP container, 10 mL min^{-1} (10% N_2/He), and 290 °C.

https://doi.org/10.1021/acs.jpcc.4c06925
J. Phys. Chem. C XXXX, XXX, XXX−XXX

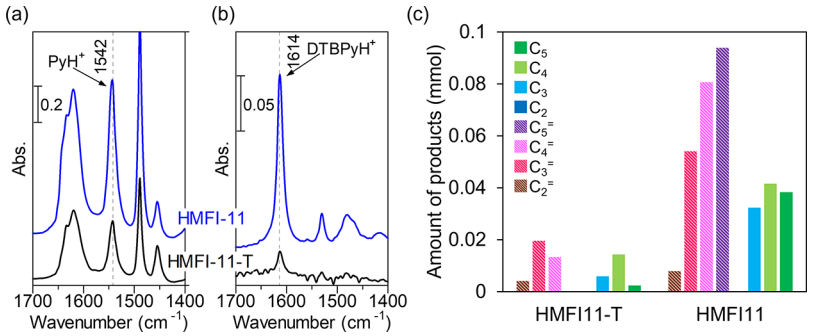

Figure 6. IR spectra of (a) Py and (b) DTBPy adsorbed on HMFI11 and HMFI11-T at 200 °C. (c) Catalytic results for PP pyrolysis under 10% N_2/He.

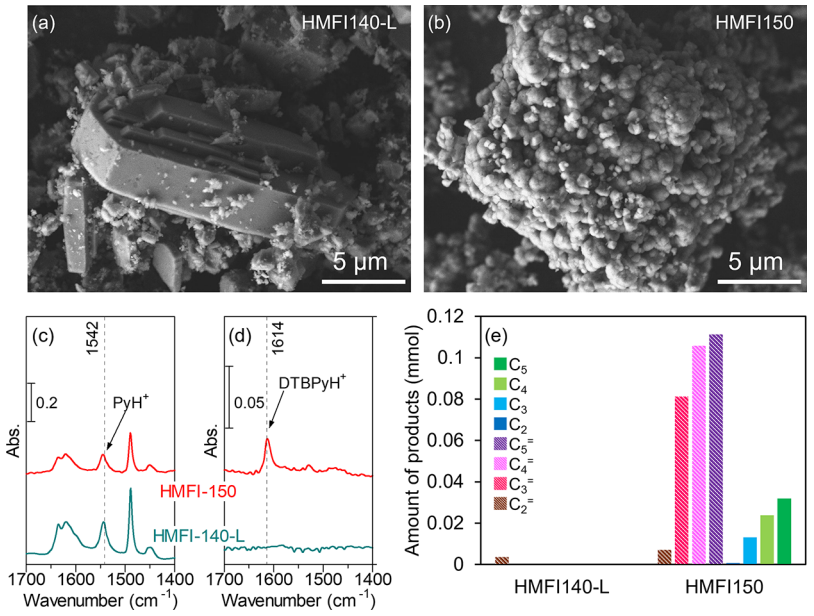

Figure 7. SEM images of (a) HMFI140-L and (b) HMFI150. IR spectra of (c) Py and (d) DTBPy adsorbed on the catalysts at 200 °C. (e) Catalytic results for PP pyrolysis using HMFI140-L and HMFI150.

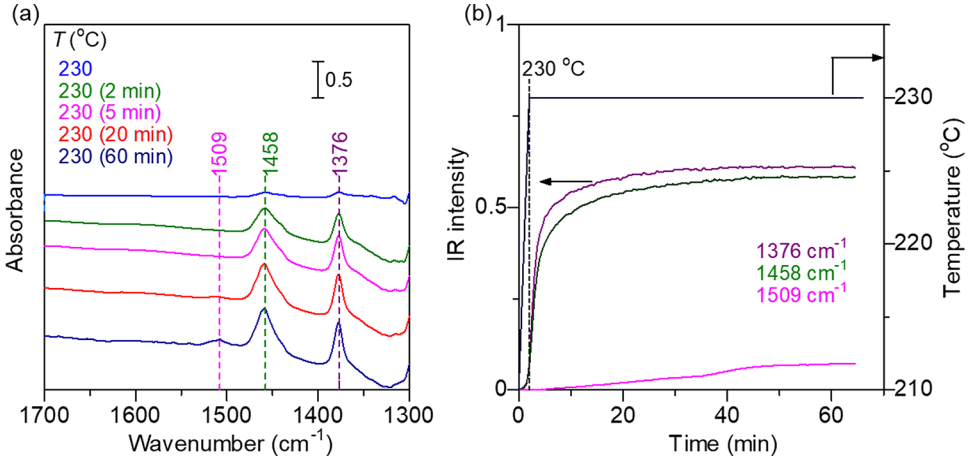

Figure 8. *Operando* IR results during PP pyrolysis on HMFI150 under He: (a) typical IR spectra 2, 5, 20, and 60 min after the addition of adsorbed species and (b) the time course of IR intensity. After the measurement of the background spectrum of the IR disk (5.2 mg of PP/46.8 mg of HMFI150 mixture) at 210 °C, the IR cell was heated to 230 °C (20 °C min^{-1} ramp rate), followed by maintaining the temperature at 230 °C.

3.3. Spectroscopic Studies on PP Depolymerization Mechanism. In most of the catalytic tests shown above, the conversions of PP (based on the decrease of the solid weight after the reaction) were larger than the total yields of hydrocarbons. The UV−vis spectra of the zeolite catalysts after the reaction suggested the presence of aromatic hydrocarbon species in the zeolites. These results suggest that part of the PP is converted not to gas-phase hydrocarbons but to solid

https://doi.org/10.1021/acs.jpcc.4c06925
J. Phys. Chem. C XXXX, XXX, XXX−XXX

or liquid hydrocarbon species in the zeolites (or on their surfaces). To identify the adsorbed hydrocarbon species, we carried out *in situ* IR experiments of the PP/zeolite mixture under He. Figure 8 shows the *in situ* IR result during the PP conversion on HMFI150 under He at 230 °C, which is higher than the melting point of PP but lower than that for gas-phase hydrocarbon formation (250−300 °C). After the measurement of the background spectrum of the IR disk (5.2 mg of PP/52 mg of HMFI150 mixture) at 210 °C under He, the IR cell was heated to 230 °C in 1 min, and then the temperature was kept at 230 °C. As the temperature reached 230 °C, two bands at 1458 and 1376 cm^{-1} were observed. Their peak intensities increased with time and leveled off above 30 min. Recently, Góra-Marek and co-workers have reported *in situ* IR spectra of adsorbed hydrocarbon species during the heating of the HMFI/PP mixture from room temperature to 250 °C under N_2 flow;[84] they observed a band at 1480−1430 cm^{-1} that is associated with an asymmetric out-of-plane CH_3 deformation and a band at 1393−1356 cm^{-1} due to a symmetric in-phase CH_3 deformation[85] of blanched hydrocarbons produced by the cracking of PP on HMFI. Given that the two bands at 1458 and 1376 cm^{-1} show similar kinetic behaviors (Figure 8), we assign these bands to asymmetric out-of-plane and symmetric in-phase CH_3 deformations. The increase in intensity of the bands at 1458 and 1376 cm^{-1} observed in this study suggests the formation of blanched hydrocarbon species containing CH_3 groups caused by the cracking of PP.

To identify the structure of the newly formed hydrocarbon species, we carried out ^1H NMR analysis of the IR disk after the experiment depicted in Figure 8. The ^1H NMR spectrum (Figure 9) shows that the alkane species on HMFI150 are

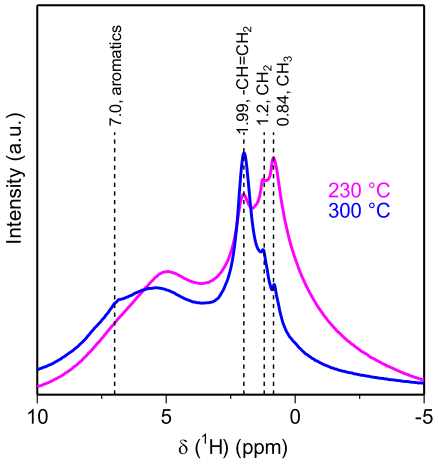

Figure 9. ^1H NMR spectra of 10 wt % PP−HMFI150 mixture after heating at 230 °C (pink) and 5 wt % PP−HMFI150 mixture after heating at 300 °C (blue) for 1 h under He flow.

composed of CH_3 group (0.84 ppm), CH_2 group (1.2 ppm), and CH_x group adjacent to the olefinic groups (1.99 ppm).[86] Given the generally accepted fact that acid-catalyzed cracking of alkanes gives an alkane and a terminal olefin, the above IR and ^1H NMR results suggest that the cracking of PP by Brønsted acid sites on external surfaces of HMFI yields an alkane and a terminal olefin adsorbed on HMFI at 230 °C. For the product of the same experiments after the reaction at a higher temperature (300 °C), the ^1H NMR signal of the CH_3 group (0.84 ppm) was further upfield than that of the CH_x group adjacent to the olefinic groups (1.99 ppm), suggesting that long-chain alkanes such as PP and oligomeric PP were converted to short-chain terminal olefins. Additionally, the signal due to light aromatics (7.0 ppm) was observed on the catalyst after PP conversion at 300 °C.

Figure 10(a) shows the dynamic changes in the *in situ* IR spectra and time dependence of the gas-phase product formation rates during the PP conversion on HMFI150 under He at 300 °C. The IR cell was heated to 300 °C for 9 min, and then the temperature was kept at 300 °C, while the IR spectra. The combination of the *in situ* IR measurement with GC analysis of the outlet gas enables the *operando* IR analysis during the PP conversion. As the temperature reached 230 °C, the bands at 1458 and 1376 cm^{-1} due to CH_3 and CH_2 species were observed. At 300 °C, the intensities of these bands first increased and then decreased with time. Ethylene ($C_2^=$), propylene ($C_3^=$), butenes ($C_4^=$), pentenes ($C_5^=$), butanes (C_4), and pentanes (C_5) were observed in the gas phase, and the formation rates of these olefins reached a maximum at 20 min, at which point, the intensity of the band at 1509 cm^{-1} assignable to the carbenium ion[87−90] reached the maximum value. These results indicate the following mechanism of PP conversion. Initially, cracking of PP by Brønsted acid sites on the external surfaces of HMFI yields an alkane and a terminal olefin adsorbed on HMFI at 230 °C. Some of the alkanes and olefins could be small enough to enter the micropores of HMFI and hence undergo further cracking by the Brønsted acid sites in internal surfaces. The cracking of the oligomeric PP by the internal Brønsted acid sites is accelerated at 300 °C, resulting in the formation of gas-phase small hydrocarbons. Some of the olefins react with each other to give the carbenium ion species, which can undergo dehydrogenation to yield aromatic species (coke deposit).

Figure 10(b) shows the results of the same *operando* IR experiment for HMFI11. The formation rates of alkanes (C_3, C_4, and C_5) for HMFI11, as well as the IR intensity of the carbenium ion (1509 cm^{-1}), are higher than those for HMFI150. In contrast, the formation rates of olefins ($C_2^=$, $C_3^=$, $C_4^=$, and $C_5^=$) for HMFI11 are lower than those for HMFI150.

The conversion of olefins to aromatic species in zeolite catalysts has been studied by *in situ* UV−vis spectroscopy.[80] Figure 11 shows the result of *operando* UV−vis during PP conversion on HMFI11 under He. When the PP/HMFI11 mixture in the *in situ* UV−vis cell was heated from 29 to 290 °C, a broad band at 441 nm and a shoulder at 600 nm appeared. The band at 441 nm is assigned to small aromatic species (e.g., naphthalene and anthracene), and the band at 600 nm is assigned to large polyaromatics.[87] Online GC analyses show the temporal formation of the hydrocarbons (mostly olefins) for 28 min. In contrast, the intensity of the UV−vis bands increased with time.

We carried out ^1H NMR and ^{13}C NMR analyses (Figure 12) of the zeolite powder after the PP conversion at 290 °C. The ^1H NMR spectrum shows the presence of light aromatics (6.5−7.4 ppm) and heavy aromatics (7.4−9.0 ppm) in the HMFI catalyst. The ^{13}C NMR spectrum also shows the presence of polyaromatic species (120−150 ppm). Combining these results with the UV−vis results allows the conclusion that light and heavy aromatics are formed possibly in the internal surfaces of the catalyst during the PP conversion at 290 °C.

3.4. DFT Study on PP Depolymerization Mechanism.

To analyze the cracking of PP oligomers within the HMFI framework, we have calculated with DFT several cracking pathways of 2,4-dimethylheptene as the shortest PP oligomer model on the internal surface of the zeolite. The choice of the

https://doi.org/10.1021/acs.jpcc.4c06925
J. Phys. Chem. C XXXX, XXX, XXX−XXX

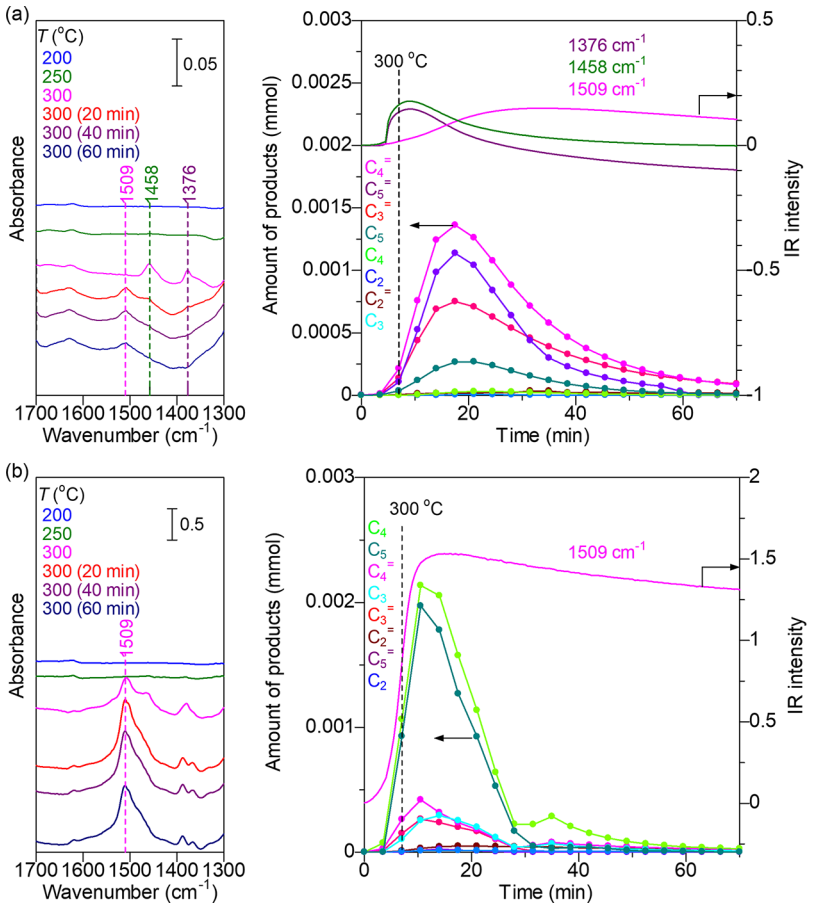

Figure 10. (a) *Operando* IR results during PP conversion on HMFI150 and (b) on HMFI11 under He: typical IR spectra of adsorbed species (left) and time course of the amount of gas products (GC analysis) and the IR intensity (right). After the measurement of the background spectrum of the IR disk (2.4 mg of PP/46 mg of HMFI150 mixture for (a), 2.5 mg of PP/46.5 mg of HMFI11 mixture for (b)) at 150 °C, the IR cell was heated to 300 °C (20 °C min^{-1} ramp rate), followed by maintaining the temperature at 300 °C.

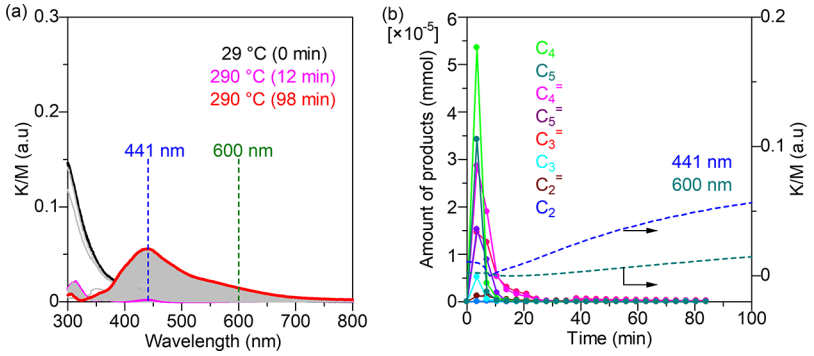

Figure 11. *Operando* UV−vis results during PP conversion on HMFI11 under He: (a) typical spectra and (b) time course of the amount of gas products (GC analysis) and the KM (441 and 600 nm). After the measurement at 29 °C, the mixed-powder sample (5.2 mg of PP, 52 mg of HMFI11) was heated to 290 °C (20 °C min^{-1}), followed by maintaining the temperature at 290 °C.

model molecule should be reasonable since the yield of isobutene was the highest among the C_4 olefin products (Figure S5). Considering the conditions of the catalytic tests, the Gibbs free energy at 563 K was applied for the energy comparison.

As shown in Figure 13, the 2,4-dimethylheptene molecule adsorbed on the internal surface of the HMFI zeolite undergoes proton transfer from the adjacent Brønsted acid site to yield a carbocation with an activation barrier of 14 kJ mol^{-1}. Various products generated via this carbocation were examined. The pathway with the lowest activation barrier was the β-scission pathway,[25] producing isobutene and a propyl alkoxide group with an activation barrier of 112 kJ mol^{-1}. Additionally, a pathway involving β-scission that produces isobutene and propylene is possible and has an activation energy of 118 kJ mol^{-1}.

The computational results suggest that the higher stability of central carbocations and the differences in activation barriers for several conversion reactions of PP oligomers favor the formation of olefins over saturated hydrocarbons, which is consistent with the reaction results.

https://doi.org/10.1021/acs.jpcc.4c06925
J. Phys. Chem. C XXXX, XXX, XXX−XXX

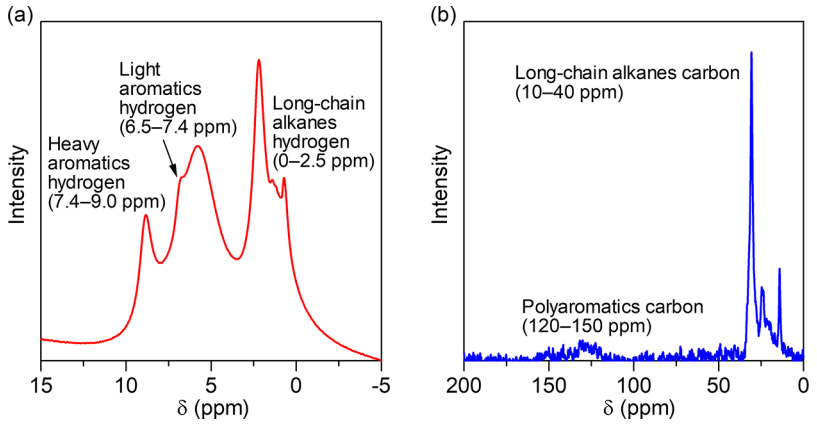

Figure 12. (a) ^{1}H NMR spectrum and (b) ^{13}C−CP-MAS NMR spectrum of the 50 wt % PP−HMFI11 mixture after heating at 290 °C for 1 h under He flow.

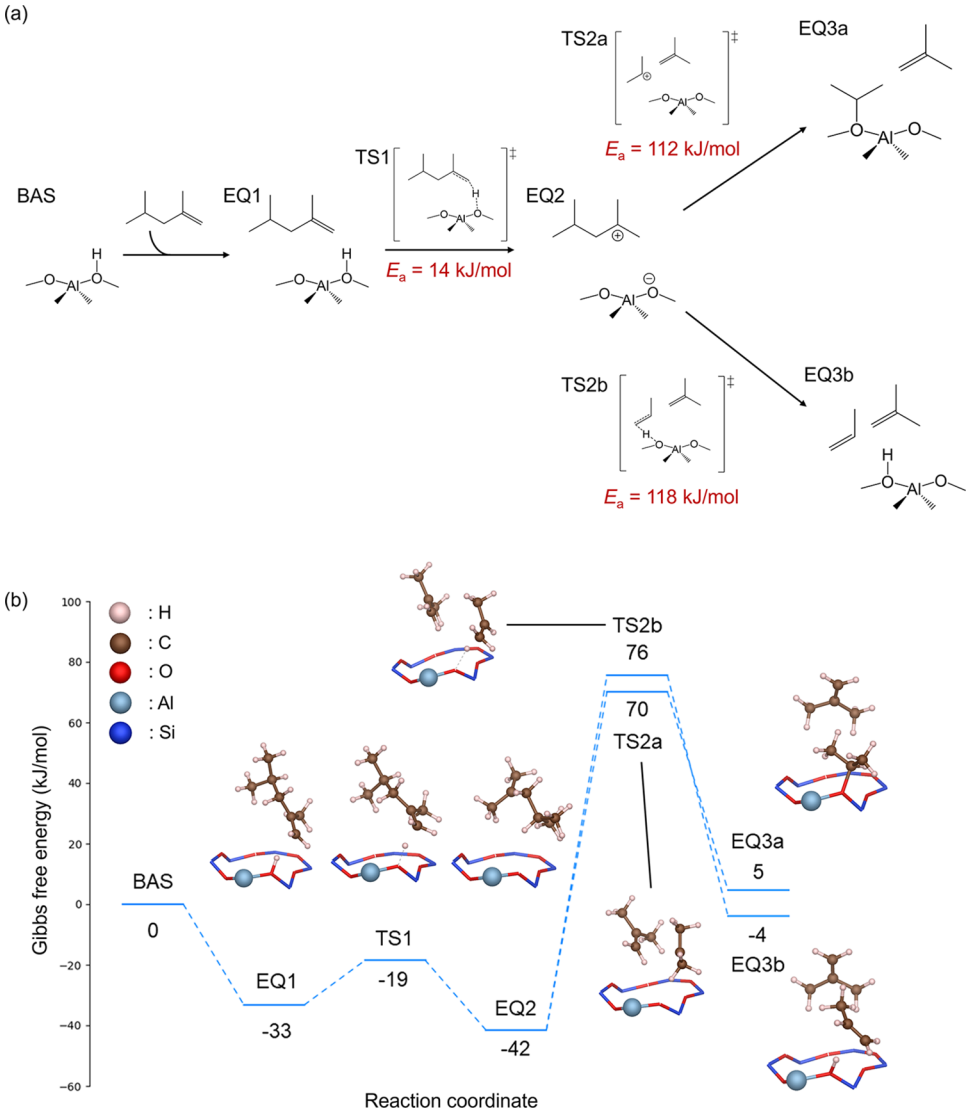

Figure 13. (a) Reaction scheme and (b) the reaction coordinate with the Gibbs free energy at 563 K for the cracking of 2,4-dimethylheptene on the Brønsted acid site of the HMFI zeolite calculated by DFT.

Based on our observations and DFT results, a plausible reaction mechanism for PP cracking is summarized in Scheme 1 as follows:[91,92] PP is first cleaved to lower-molecular-weight oligomers on external Brønsted acid sites on the HMFI zeolite. The oligomers diffuse into the pores of the HMFI zeolite and undergo cracking on the internal Brønsted acid sites, where they are cleaved into lower-molecular-weight olefins. Some of these olefins react further to form carbenium ions, which are regarded

https://doi.org/10.1021/acs.jpcc.4c06925
J. Phys. Chem. C XXXX, XXX, XXX−XXX

Scheme 1. Proposed Mechanism for the Catalytic Cracking of PP over HMFI Zeolite under He

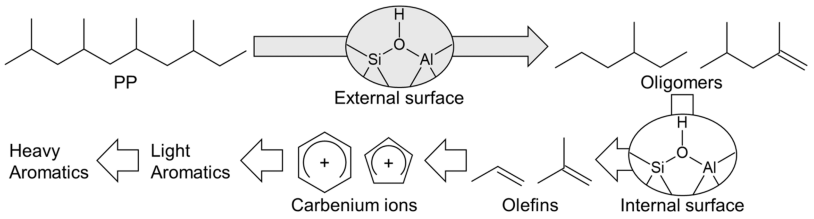

as precursors to aromatic compounds, leading to the formation of light aromatics and subsequently heavy aromatics.

4. CONCLUSIONS

HMFI effectively catalyzed the depolymerization of polypropylene into light (C_2–C_5) hydrocarbons (especially light olefins) below the pyrolytic temperature (290 °C) under a flow of inert gas. The present method is applicable to the upcycling of a model PP waste into light hydrocarbons. The Brønsted acid sites on the external surfaces of HMFI are indispensable for PP conversion and would be active sites for the cracking of PP into short-chain (oligomeric) hydrocarbon species. Adopting 2,4-dimethylheptene as an oligomeric species, a reaction pathway was proposed in light of the Gibbs free energies calculated in DFT analyses. The β-scission of 2,4-dimethylheptene by a Brønsted acid site yields isobutene and propylene (or a propyl alkoxide group) via carbocation intermediates with an activation energy below 118 kJ mol^{-1}. Some of the olefins are further converted to light and heavy aromatics (coke deposit), probably via carbenium ion species.

■ ASSOCIATED CONTENT

Supporting Information

The Supporting Information is available free of charge at https://pubs.acs.org/doi/10.1021/acs.jpcc.4c06925.

Schematics of an *operando* UV–vis/IR experiments; schematic of an *operando* diffuse reflectance UV–vis spectroscopy; result of temperature-programmed oxidation (TPO) experiment; and detailed product yield (PDF)

■ AUTHOR INFORMATION

Corresponding Authors

Akihiko Anzai – *Institute for Catalysis, Hokkaido University, Sapporo 001-0021 Hokkaido, Japan*; Email: anzai.akihiko@cat.hokudai.ac.jp

Ken-ichi Shimizu – *Institute for Catalysis, Hokkaido University, Sapporo 001-0021 Hokkaido, Japan*; orcid.org/0000-0003-0501-0294; Email: kshimizu@cat.hokudai.ac.jp

Authors

Yuriko Ando – *Institute for Catalysis, Hokkaido University, Sapporo 001-0021 Hokkaido, Japan*

Takumi Miyakage – *Institute for Catalysis, Hokkaido University, Sapporo 001-0021 Hokkaido, Japan*

Mengwen Huang – *Institute for Catalysis, Hokkaido University, Sapporo 001-0021 Hokkaido, Japan*

Abdellah Ait El Fakir – *Institute for Catalysis, Hokkaido University, Sapporo 001-0021 Hokkaido, Japan*; orcid.org/0000-0003-0549-7397

Takashi Toyao – *Institute for Catalysis, Hokkaido University, Sapporo 001-0021 Hokkaido, Japan*; orcid.org/0000-0002-6062-5622

Yuta Nakasaka – *Division of Applied Chemistry, Faculty of Engineering, Hokkaido University, Sapporo 060-8628 Hokkaido, Japan*

Alisa Phuekphong – *School of Energy Science and Engineering, Vidyasirimedhi Institute of Science and Technology, Wangchan 21210 Rayong, Thailand*; orcid.org/0000-0001-7701-0635

Makoto Ogawa – *School of Energy Science and Engineering, Vidyasirimedhi Institute of Science and Technology, Wangchan 21210 Rayong, Thailand*; orcid.org/0000-0002-3781-2016

Alexander A. Kolganov – *Department of Chemical Engineering, Faculty of Applied Sciences, Delft University of Technology, Delft 2629 HZ, The Netherlands*; orcid.org/0000-0002-0262-8892

Evgeny A. Pidko – *Department of Chemical Engineering, Faculty of Applied Sciences, Delft University of Technology, Delft 2629 HZ, The Netherlands*; orcid.org/0000-0001-9242-9901

Complete contact information is available at: https://pubs.acs.org/10.1021/acs.jpcc.4c06925

Author Contributions

Y.A. designed the experiments, performed most of the experimental investigations, and conducted the data analysis with the help of K.S., A.P., M.H., M.O., and A.A. Y.N. prepared the large crystalline HMFI zeolite sample. T.M. performed DFT calculations and wrote the draft of the DFT calculation section with the help of A.K. and E.P. K.S. and Y.A. wrote the draft, and A.A. and T.T. modified the manuscript. Finally, all authors approved the final manuscript.

Notes

The authors declare no competing financial interest.

■ ACKNOWLEDGMENTS

This work was supported by "Nanotechnology Platform Program" of the Ministry of Education, Culture, Sports, Science and Technology (MEXT), Japan, Grant Number JPMXP09A21HK0027. This study was financially supported by KAKENHI (Grant Nos. 21H04626 22H01868, 23H01997, and 23K20034) from Japan Society for the Promotion of Science (JSPS). This study was also supported by the Joint Usage/Research Center for Catalysis. A.A.K. and E.A.P. thank the NWO Domein Exacte en Natuurwetenschappen for the use of the Dutch national supercomputer, Snellius.

■ REFERENCES

(1) Geyer, R.; Jambeck, J. R.; Law, K. L. Production, Use, and Fate of All Plastics Ever Made. *Sci. Adv.* **2017**, 3 (7), No. e1700782.

(2) Hundertmark, T.; Mayer, M.; McNally, C.; Simons, T. J.; Witte, C. How Plastics-Waste Recycling Could Transform the Chemical Industry. *McKinsey on Chemicals*; 2018.
(3) Marquez, C.; Martin, C.; Linares, N.; De Vos, D. Catalytic Routes towards Polystyrene Recycling. *Mater. Horiz.* **2023**, *10*, 1625−1640.
(4) Vollmer, I.; Jenks, M. J. F.; Roelands, M. C. P.; White, R. J.; van Harmelen, T.; de Wild, P.; van der Laan, G. P.; Meirer, F.; Keurentjes, J. T. F.; Weckhuysen, B. M. Beyond Mechanical Recycling: Giving New Life to Plastic Waste. *Angew. Chem., Int. Ed.* **2020**, *59* (36), 15402−15423.
(5) Kaminsky, W. Chemical Recycling of Plastics by Fluidized Bed Pyrolysis. *Fuel Commun.* **2021**, *8*, No. 100023.
(6) Wang, N. M.; Strong, G.; Dasilva, V.; Gao, L.; Huacuja, R.; Konstantinov, I. A.; Rosen, M. S.; Nett, A. J.; Ewart, S.; Geyer, R.; et al. Chemical Recycling of Polyethylene by Tandem Catalytic Conversion to Propylene. *J. Am. Chem. Soc.* **2022**, *144* (40), 18526−18531.
(7) Nishida, H. Development of Materials and Technologies for Control of Polymer Recycling. *Polym. J.* **2011**, *43*, 435−447.
(8) Castéran, F.; Delage, K.; Hascoët, N.; Ammar, A.; Chinesta, F.; Cassagnau, P. Data-Driven Modelling of Polyethylene Recycling under High-Temperature Extrusion. *Polymers* **2022**, *14* (4), 800.
(9) Su, J.; Xu, G.; Dong, B.; Yang, R.; Sun, H.; Wang, Q. Closed-Loop Chemical Recycling of Poly(ϵ-Caprolactone) by Tuning Reaction Parameters. *Polym. Chem.* **2022**, *13* (41), 5897−5904.
(10) Zou, L.; Xu, R.; Wang, H.; Wang, Z.; Sun, Y.; Li, M. Chemical Recycling of Polyolefins: A Closed-Loop Cycle of Waste to Olefins. *Natl. Sci. Rev.* **2023**, *10* (9), No. nwad207.
(11) Lin, Y. H.; Yang, M. H. Tertiary Recycling of Polyethylene Waste by Fluidised-Bed Reactions in the Presence of Various Cracking Catalysts. *J. Anal. Appl. Pyrolysis* **2008**, *83* (1), 101−109.
(12) Kim, D. H.; Han, D. O.; In Shim, K.; Kim, J. K.; Pelton, J. G.; Ryu, M. H.; Joo, J. C.; Han, J. W.; Kim, H. T.; Kim, K. H. One-Pot Chemo-Bioprocess of PET Depolymerization and Recycling Enabled by a Biocompatible Catalyst, Betaine. *ACS Catal.* **2021**, *11* (7), 3996−4008.
(13) Ragaert, K.; Delva, L.; Van Geem, K. Mechanical and Chemical Recycling of Solid Plastic Waste. *Waste Manage.* **2017**, *69*, 24−58.
(14) Kang, Q.; Chu, M.; Xu, P.; Wang, X.; Wang, S.; Cao, M.; Ivasenko, O.; Sham, T. K.; Zhang, Q.; Sun, Q.; Chen, J. Entropy Confinement Promotes Hydrogenolysis Activity for Polyethylene Upcycling. *Angew. Chem., Int. Ed.* **2023**, *62* (47), No. e202313174.
(15) Celik, G.; Kennedy, R. M.; Hackler, R. A.; Ferrandon, M.; Tennakoon, A.; Patnaik, S.; Lapointe, A. M.; Ammal, S. C.; Heyden, A.; Perras, F. A.; et al. Upcycling Single-Use Polyethylene into High-Quality Liquid Products. *ACS Cent. Sci.* **2019**, *5* (11), 1795−1803.
(16) Wei, J.; Liu, J.; Zeng, W.; Dong, Z.; Song, J.; Liu, S.; Liu, G. Catalytic Hydroconversion Processes for Upcycling Plastic Waste to Fuels and Chemicals. *Catal. Sci. Technol.* **2023**, *13*, 1258−1280.
(17) Zhang, F.; Zeng, M.; Yappert, R. D.; Sun, J.; Lee, Y.-H.; Lapointe, A. M.; Peters, B.; Abu-Omar, M. M.; Scott, S. L. Polyethylene Upcycling to Long-Chain Alkylaromatics by Tandem Hydrogenolysis/Aromatization. *Science* **2020**, *370* (6515), 437−441.
(18) Lv, H.; Huang, F.; Zhang, F. Upcycling Waste Plastics with a C−C Backbone by Heterogeneous Catalysis. *Langmuir* **2024**, *40* (10), 5077−5089.
(19) Zhang, W.; Yao, H.; Khare, R.; Zhang, P.; Yang, B.; Hu, W.; Ray, D.; Hu, J.; Camaioni, D. M.; Wang, H.; et al. Chloride and Hydride Transfer as Keys to Catalytic Upcycling of Polyethylene into Liquid Alkanes. *Angew. Chem., Int. Ed.* **2024**, *63* (17), No. e202319580.
(20) Zhang, W.; Kim, S.; Wahl, L.; Khare, R.; Hale, L.; Hu, J.; Camaioni, D. M.; Gutiérrez, O. Y.; Liu, Y.; Lercher, J. A. Low-Temperature Upcycling of Polyolefins into Liquid Alkanes via Tandem Cracking-Alkylation. *Science* **2023**, *379* (6634), 807−811.
(21) Chen, L.; Meyer, L. C.; Kovarik, L.; Meira, D.; Pereira-Hernandez, X. I.; Shi, H.; Khivantsev, K.; Gutiérrez, O. Y.; Szanyi, J. Disordered, Sub-Nanometer Ru Structures on CeO_2 are Highly Efficient and Selective Catalysts in Polymer Upcycling by Hydrogenolysis. *ACS Catal.* **2022**, *12* (8), 4618−4627.
(22) Miura, H.; Doi, M.; Yasui, Y.; Masaki, Y.; Nishio, H.; Shishido, T. Diverse Alkyl−Silyl Cross-Coupling via Homolysis of Unactivated C(sp^3)-O Bonds with the Cooperation of Gold Nanoparticles and Amphoteric Zirconium Oxides. *J. Am. Chem. Soc.* **2023**, *145* (8), 4613−4625.
(23) Chen, W.; Jiao, Y.; Liu, Y.; Wang, M.; Zhang, F.; Ma, D. One-Pot Upgrading Polyethylene and CO_2 to Aromatics via Tandem Catalysis. *CCS Chem.* **2024**, *6* (6), 1422−1429.
(24) Liang, X.; Wang, M.; Ma, D. One-Pot Conversion of Polyester and Carbonate into Formate without External H_2. *J. Am. Chem. Soc.* **2024**, *146* (4), 2711−2717.
(25) Duan, J.; Chen, W.; Wang, C.; Wang, L.; Liu, Z.; Yi, X.; Fang, W.; Wang, H.; Wei, H.; Xu, S.; et al. Coking-Resistant Polyethylene Upcycling Modulated by Zeolite Micropore Diffusion. *J. Am. Chem. Soc.* **2022**, *144* (31), 14269−14277.
(26) Rejman, S.; Vollmer, I.; Werny, M. J.; Vogt, E. T. C.; Meirer, F.; Weckhuysen, B. M. Transport Limitations in Polyolefin Cracking at the Single Catalyst Particle Level. *Chem. Sci.* **2023**, *14* (37), 10068−10080.
(27) Tsubota, S.; Kokuryo, S.; Miyake, K.; Uchida, Y.; Mizusawa, A.; Kubo, T.; Nishiyama, N. Understanding the Role of the Surface Acidity of MFI Zeolites during LDPE Cracking: Decomposition Temperature and Product Distribution. *ACS Catal.* **2024**, *14*, 18145−18155.
(28) Tsubota, S.; Kokuryo, S.; Tamura, K.; Miyake, K.; Uchida, Y.; Mizusawa, A.; Kubo, T.; Nishiyama, N. Exploring the Effect of Brønsted Acidity of MFI-Type Zeolites on Catalytic Cracking Temperature of Low Density Polyethylene. *Catal. Sci. Technol.* **2024**, *14* (5), 1369−1374.
(29) Xu, Z.; Eric Munyaneza, N.; Zhang, Q.; Sun, M.; Posada, C.; Venturo, P.; Rorrer, N. A.; Miscall, J.; Sumpter, B. G.; Liu, G. Chemical Upcycling of Polyethylene, Polypropylene, and Mixtures to High-Value Surfactants. *Science* **2023**, *381* (6658), 666−671.
(30) Serrano, D. P.; Aguado, J.; Escola, J. M. Developing Advanced Catalysts for the Conversion of Polyolefinic Waste Plastics into Fuels and Chemicals. *ACS Catal.* **2012**, *2* (9), 1924−1941.
(31) Lopez, G.; Artetxe, M.; Amutio, M.; Bilbao, J.; Olazar, M. Thermochemical Routes for the Valorization of Waste Polyolefinic Plastics to Produce Fuels and Chemicals. A Review. *Renewable Sustainable Energy Rev.* **2017**, *73*, 346−368.
(32) Yuan, H.; Li, C.; Shan, R.; Zhang, J.; Wu, Y.; Chen, Y. Recent Developments on the Zeolites Catalyzed Polyolefin Plastics Pyrolysis. *Fuel Process. Technol.* **2022**, *238*, No. 107531.
(33) Uemichi, Y.; Ayame, A.; Yoshida, T.; Kanoh, H. Gasification of Polyethylene over Solid Catalysts (Part 4) Gasification over Sodium X Zeolite and Silica−Alumina in a Fixed Bed Tubular Flow Reactor. *J. Jpn. Pet. Inst.* **1980**, *23* (1), 35−43.
(34) Ishihara, Y.; Nanbu, H.; Lkemura, T.; Takesue, T. Catalytic Decomposition of Polyethylene Using a Tubular Flow Reactor System. *Fuel* **1990**, *69* (8), 978−984.
(35) Ohkita, H.; Nishiyama, R.; Tochihara, Y.; Mizushima, T.; Kakuta, N.; Morioka, Y.; Ueno, A.; Namiki, Y.; Tanifuji, S.; Katoh, H.; et al. Acid Properties of Silica-Alumina Catalysts and Catalytic Degradation of Polyethylene. *Ind. Eng. Chem. Res.* **1993**, *32*, 3112−3116.
(36) Songip, A. R.; Masuda, T.; Kuwahara, H.; Hashimoto, K. Production of High-Quality Gasoline by Catalytic Cracking over Rare-Earth Metal Exchanged Y-Type Zeolites of Heavy Oil from Waste Plastics. *Energy Fuels* **1994**, *8* (1), 136−140.
(37) Garforth, A. A.; Lin, Y.-H.; Sharratt, P. N.; Dwyer, J. Production of Hydrocarbons by Catalytic Degradation of High-Density Polyethylene in a Laboratory fluidised-Bed Reactor. *Appl. Catal., A* **1998**, *169* (2), 331−342.
(38) Saha, B.; Ghoshal, A. K. Hybrid Genetic Algorithm and Model-Free Coupled Direct Search Methods for Pyrolysis Kinetics of ZSM-5 Catalyzed Decomposition of Waste Low-Density Polyethylene. *Ind. Eng. Chem. Res.* **2007**, *46* (17), 5485−5492.
(39) Nishino, J.; Itoh, M.; Fujiyoshi, H.; Uemichi, Y. Catalytic Degradation of Plastic Waste into Petrochemicals Using Ga-ZSM-5. *Fuel* **2008**, *87* (17−18), 3681−3686.
(40) Serrano, D. P.; Aguado, J.; Escola, J. M.; Rodriguez, J. M.; Peral, A. Catalytic Properties in Polyolefin Cracking of Hierarchical Nanocrystalline HZSM-5 Samples Prepared According to Different Strategies. *J. Catal.* **2010**, *276* (1), 152−160.

https://doi.org/10.1021/acs.jpcc.4c06925
J. Phys. Chem. C XXXX, XXX, XXX−XXX

(41) Artetxe, M.; Lopez, G.; Amutio, M.; Elordi, G.; Bilbao, J.; Olazar, M. Cracking of High Density Polyethylene Pyrolysis Waxes on HZSM-5 Catalysts of Different Acidity. *Ind. Eng. Chem. Res.* **2013**, *52* (31), 10637−10645.
(42) Chen, Z.; Zhang, X.; Yang, F.; Peng, H.; Zhang, X.; Zhu, S.; Che, L. Deactivation of a Y-Zeolite Based Catalyst with Coke Evolution during the Catalytic Pyrolysis of Polyethylene for Fuel Oil. *Appl. Catal., A* **2021**, *609*, No. 117873.
(43) Klaimy, S.; Ciotonea, C.; Dhainaut, J.; Royer, S.; Casetta, M.; Duquesne, S.; Tricot, G.; Lamonier, J. F. Flash Catalytic Pyrolysis of Polyethylene over (Alumino)silicate Materials. *ChemCatChem* **2020**, *12* (4), 1109−1116.
(44) Wang, W.; Yao, C.; Ge, X.; Pu, X.; Yuan, J.; Sun, W.; Chen, W.; Feng, X.; Qian, G.; Duan, X.; et al. Catalytic Conversion of Polyethylene into Aromatics with Pt/ZSM-5: Insights into Reaction Pathways and Rate-Controlling Step Regulation. *J. Mater. Chem. A* **2023**, *11* (27), 14933−14940.
(45) Wang, C.; Xie, T.; Kots, P. A.; Vance, B. C.; Yu, K.; Kumar, P.; Fu, J.; Liu, S.; Tsilomelekis, G.; Stach, E. A.; et al. Polyethylene Hydrogenolysis at Mild Conditions over Ruthenium on Tungstated Zirconia. *JACS Au* **2021**, *1* (9), 1422−1434.
(46) Liu, S.; Kots, P. A.; Vance, B. C.; Danielson, A.; Vlachos, D. G. Plastic Waste to Fuels by Hydrocracking at Mild Conditions. *Sci. Adv.* **2021**, *7* (17), No. eabf8283.
(47) Tamura, M.; Miyaoka, S.; Nakaji, Y.; Tanji, M.; Kumagai, S.; Nakagawa, Y.; Yoshioka, T.; Tomishige, K. Structure-Activity Relationship in Hydrogenolysis of Polyolefins over Ru/Support Catalysts. *Appl. Catal., B* **2022**, *318*, No. 121870.
(48) Miller, J. H.; Starace, A. K.; Ruddy, D. A. Catalytic Activation of Polyethylene Model Compounds Over Metal-Exchanged Beta Zeolites. *ChemSusChem* **2022**, *15* (12), No. e202200535.
(49) Mason, A. H.; Motta, A.; Das, A.; Ma, Q.; Bedzyk, M. J.; Kratish, Y.; Marks, T. J. Rapid Atom-Efficient Polyolefin Plastics Hydrogenolysis Mediated by a Well-Defined Single-Site Electrophilic/Cationic Organo-Zirconium Catalyst. *Nat. Commun.* **2022**, *13* (1), No. 7187.
(50) Wang, H.; Yoskamtorn, T.; Zheng, J.; Ho, P. L.; Ng, B.; Tsang, S. C. E. Ce-Promoted PtSn-Based Catalyst for Hydrocracking of Polyolefin Plastic Waste into High Yield of Gasoline-Range Products. *ACS Catal.* **2023**, *13* (24), 15886−15898.
(51) Zhou, Q.; Wang, D.; Wang, Q.; He, K.; Lim, K. H.; Yang, X.; Wang, W. J.; Li, B. G.; Liu, P. Mechanistic Understanding of Efficient Polyethylene Hydrocracking over Two-Dimensional Platinum-Anchored Tungsten Trioxide. *Angew. Chem., Int. Ed.* **2023**, *62* (40), No. e202305644.
(52) Jia, X.; Qin, C.; Friedberger, T.; Guan, Z.; Huang, Z. Efficient and Selective Degradation of Polyethylenes into Liquid Fuels and Waxes under Mild Conditions. *Sci. Adv.* **2016**, *2* (6), No. e1501591.
(53) Chen, S.; Tennakoon, A.; You, K. E.; Paterson, A. L.; Yappert, R.; Alayoglu, S.; Fang, L.; Wu, X.; Zhao, T. Y.; Lapak, M. P.; et al. Ultrasmall Amorphous Zirconia Nanoparticles Catalyse Polyolefin Hydrogenolysis. *Nat. Catal.* **2023**, *6* (2), 161−173.
(54) Tan, J. Z.; Hullfish, C. W.; Zheng, Y.; Koel, B. E.; Sarazen, M. L. Conversion of Polyethylene Waste to Short Chain Hydrocarbons under Mild Temperature and Hydrogen Pressure with Metal-Free and Metal-Loaded MFI Zeolites. *Appl. Catal., B* **2023**, *338*, No. 123028.
(55) Lee, J. Y.; Park, S. M.; Saha, S. K.; Cho, S. J.; Seo, G. Liquid-Phase Degradation of Polyethylene (PE) over MFI Zeolites with Mesopores: Effects of the Structure of PE and the Characteristics of Mesopores. *Appl. Catal., B* **2011**, *108*−*109*, 61−71.
(56) Pennel, M. L.; Maurya, A. K.; Ebrahim, A. M.; Tassone, C. J.; Cargnello, M. Activity of Silica-Alumina for the Conversion of Polyethylene into Tunable Aromatics Below Pyrolytic Temperatures. *ACS Sustainable Chem. Eng.* **2023**, *11* (34), 12623−12630.
(57) Zhang, Z.; Chen, H.; Li, G.; Hu, W.; Niu, B.; Long, D.; Zhang, Y. Highly Selective Upgrading of Polyethylene into Light Aromatics via a Low-Temperature Melting-Catalysis Strategy. *ACS Catal.* **2024**, *14* (4), 2552−2561.
(58) Vollmer, I.; Jenks, M. J. F.; Rejman, S.; Meirer, F.; Gurinov, A.; Baldus, M.; Weckhuysen, B. M. Unravelling Potential Reaction Intermediates during Catalytic Pyrolysis of Polypropylene with Microscopy and Spectroscopy. *Catal. Sci. Technol.* **2024**, *14* (4), 894−902.
(59) Tago, T.; Konno, H.; Nakasaka, Y.; Masuda, T. Size-Controlled Synthesis of Nano-Zeolites and Their Application to Light Olefin Synthesis. *Catal. Surv. Asia* **2012**, *16*, 148−163.
(60) Kühne, T. D.; Iannuzzi, M.; Del Ben, M.; Rybkin, V. V.; Seewald, P.; Stein, F.; Laino, T.; Khaliullin, R. Z.; Schütt, O.; Schiffmann, F.; Golze, D.; et al. CP2K: An Electronic Structure and Molecular Dynamics Software Package - Quickstep: Efficient and Accurate Electronic Structure Calculations. *J. Chem. Phys.* **2020**, *152* (19), No. 194103.
(61) Baerlocher, C.; McCusker, L. B.; Hanson, R. *Database of Zeolite Structures*; https://www.iza-structure.org/databases/.
(62) Ghorbanpour, A.; Rimer, J. D.; Grabow, L. C. Periodic, vdW-Corrected Density Functional Theory Investigation of the Effect of Al Siting in H-ZSM-5 on Chemisorption Properties and Site-Specific Acidity. *Catal. Commun.* **2014**, *52*, 98−102.
(63) Perdew, J. P.; Burke, K.; Ernzerhof, M. Generalized Gradient Approximation Made Simple. *Phys. Rev. Lett.* **1996**, *77* (18), 3865−3868.
(64) Grimme, S.; Antony, J.; Ehrlich, S.; Krieg, H. A Consistent and Accurate Ab Initio Parametrization of Density Functional Dispersion Correction (DFT-D) for the 94 Elements H-Pu. *J. Chem. Phys.* **2010**, *132* (15), No. 154104.
(65) Grimme, S.; Ehrlich, S.; Goerigk, L. Effect of the Damping Function in Dispersion Corrected Density Functional Theory. *J. Comput. Chem.* **2011**, *32* (7), 1456−1465.
(66) Goedecker, S.; Teter, M.; Hutter, J. Separable Dual-Space Gaussian Pseudopotentials. *Phys. Rev. B* **1996**, *54* (3), 1703.
(67) Hartwigsen, C.; Goedecker, S.; Hutter, J. Relativistic Separable Dual-Space Gaussian Pseudopotentials from H to Rn. *Phys. Rev. B* **1998**, *58* (7), 3641−3662.
(68) VandeVondele, J.; Hutter, J. An Efficient Orbital Transformation Method for Electronic Structure Calculations. *J. Chem. Phys.* **2003**, *118* (10), 4365−4369.
(69) Broyden, C. G. The Convergence of a Class of Double-Rank Minimization Algorithms 1. General Considerations. *IMA J. Appl. Math.* **1970**, *6* (1), 76−90.
(70) Fletcher, R. A New Approach to Variable Metric Algorithms. *Comput. J.* **1970**, *13* (3), 317−322.
(71) Goldfarb, D. A Family of Variable-Metric Methods Derived by Variational Means. *Math. Comput.* **1970**, *24* (109), 23−26.
(72) Shanno, D. F. Conditioning of Quasi-Newton Methods for Function Minimization. *Math. Comput.* **1970**, *24* (111), 647−656.
(73) Henkelman, G.; Uberuaga, B. P.; Jónsson, H. A Climbing Image Nudged Elastic Band Method for Finding Saddle Points and Minimum Energy Paths. *J. Chem. Phys.* **2000**, *113* (22), 9901−9904.
(74) Kästner, J.; Sherwood, P. Superlinearly Converging Dimer Method for Transition State Search. *J. Chem. Phys.* **2008**, *128* (1), No. 014106.
(75) Henkelman, G.; Jónsson, H. Improved Tangent Estimate in the Nudged Elastic Band Method for Finding Minimum Energy Paths and Saddle Points. *J. Chem. Phys.* **2000**, *113* (22), 9978−9985.
(76) Chaffey-Millar, H.; Nikodem, A.; Matveev, A. V.; Krüger, S.; Rösch, N. Improving upon String Methods for Transition State Discovery. *J. Chem. Theory Comput.* **2012**, *8* (2), 777−786.
(77) Cramer, C. J. *Essentials of Computational Chemistry: Theories and Models*, 2nd ed.; Wiley, 2004.
(78) Ochterski, J. W. *Thermochemistry in Gaussian*; Gaussian, Inc., 2000.
(79) De Moor, B. A.; Reyniers, M. F.; Marin, G. B. Physisorption and Chemisorption of Alkanes and Alkenes in H-FAU: A Combined Ab Initio-Statistical Thermodynamics Study. *Phys. Chem. Chem. Phys.* **2009**, *11* (16), 2939−2958.
(80) Fu, D.; van der Heijden, O.; Stanciakova, K.; Schmidt, J. E.; Weckhuysen, B. M. Disentangling Reaction Processes of Zeolites within

https://doi.org/10.1021/acs.jpcc.4c06925
J. Phys. Chem. C XXXX, XXX, XXX−XXX

Single-Oriented Channels. *Angew. Chem. Int. Ed.* **2020**, *59* (36), 15502−15506.
(81) Dai, L.; Zhou, N.; Li, H.; Wang, Y.; Liu, Y.; Cobb, K.; Cheng, Y.; Lei, H.; Chen, P.; Ruan, R. Catalytic Fast Pyrolysis of Low Density Polyethylene into Naphtha with High Selectivity by Dual-Catalyst Tandem Catalysis. *Sci. Total Environ.* **2021**, *771*, No. 144995.
(82) Zheng, S.; Heydenrych, H. R.; Röger, H. P.; Jentys, A.; Lercher, J. A. On the Enhanced Selectivity of HZSM-5 Modified by Chemical Liquid Deposition. *Top. Catal.* **2003**, *22* (1−2), 101−106.
(83) Konno, H.; Okamura, T.; Kawahara, T.; Nakasaka, Y.; Tago, T.; Masuda, T. Kinetics of N-Hexane Cracking over ZSM-5 Zeolites - Effect of Crystal Size on Effectiveness Factor and Catalyst Lifetime. *Chem. Eng. J.* **2012**, *207−208*, 490−496.
(84) Tarach, K. A.; Akouche, M.; Pyra, K.; Valtchev, V.; Jajko, G.; Gilson, J. P.; Góra-Marek, K. Polypropylene Cracking on Embryonic and ZSM-5 Catalysts − An Operando Study. *Appl. Catal., B* **2023**, *334*, No. 122871.
(85) Lamberti, C.; Groppo, E.; Spoto, G.; Bordiga, S.; Zecchina, A. Infrared Spectroscopy of Transient Surface Species. *Adv. Catal.* **2007**, *51*, 1−74.
(86) Feller, A.; Barth, J. O.; Guzman, A.; Zuazo, I.; Lercher, J. A. Deactivation Pathways in Zeolite-Catalyzed Isobutane/Butene Alkylation. *J. Catal.* **2003**, *220* (1), 192−206.
(87) Mores, D.; Kornatowski, J.; Olsbye, U.; Weckhuysen, B. M. Coke Formation during the Methanol-to-Olefin Conversion: In Situ Microspectroscopy on Individual H-ZSM-5 Crystals with Different Brønsted Acidity. *Chem. - Eur. J.* **2011**, *17* (10), 2874−2884.
(88) Kiricsi, I.; Förster, H.; Tasi, G.; Nagy, J. B. Generation, Characterization, and Transformations of Unsaturated Carbenium Ions in Zeolites. *Chem. Rev.* **1999**, *99* (11), 2085−2114.
(89) Hernandez, E. D.; Jentoft, F. C. Spectroscopic Signatures Reveal Cyclopentenyl Cation Contributions in Methanol-to-Olefins Catalysis. *ACS Catal.* **2020**, *10* (10), 5764−5782.
(90) Maggiulli, L.; Sushkevich, V. L.; Kröcher, O.; van Bokhoven, J. A.; Ferri, D. Correlating the Nature of Carbenium Ions in Zeolites to the Product Distribution in the Methanol-to-Olefins Process. *ACS Catal.* **2024**, *14* (15), 11477−11489.
(91) Greensfelder, B. S.; Voge, H. H.; Good, G. M. Catalytic and Thermal Cracking of Pure Hydrocarbons: Mechanisms of Reaction. *Ind. Eng. Chem.* **1949**, *41* (11), 2573−2584.
(92) Thomas, C. L. Chemistry of Cracking Catalysts. *Ind. Eng. Chem.* **1949**, *41* (11), 2564−2573.

https://doi.org/10.1021/acs.jpcc.4c06925
J. Phys. Chem. C XXXX, XXX, XXX−XXX